

Unharmful Backdoor-based Client-side Watermarking in Federated Learning

Kaijing Luo
Huawei Cloud
Shenzhen, China

Ka-Ho Chow*
The University of Hong Kong
Hong Kong, China

Abstract—Protecting intellectual property (IP) in federated learning (FL) is increasingly important as clients contribute proprietary data to collaboratively train models. Model watermarking, particularly through backdoor-based methods, has emerged as a popular approach for verifying ownership and contributions in deep neural networks trained via FL. By manipulating their datasets, clients can embed a secret pattern, resulting in non-intuitive predictions that serve as proof of participation, useful for claiming incentives or IP co-ownership. However, this technique faces practical challenges: client watermarks can collide, leading to ambiguous ownership claims, and malicious clients may exploit watermarks to inject harmful backdoors, jeopardizing model integrity. To address these issues, we propose Sanitizer, a server-side method that ensures client-embedded backdoors cannot be triggered on natural queries in harmful ways. It identifies subnets within client-submitted models, extracts backdoors throughout the FL process, and confines them to harmless, client-specific input subspaces. This approach not only enhances Sanitizer’s efficiency but also resolves conflicts when clients use similar triggers with different target labels. Our empirical results demonstrate that Sanitizer achieves near-perfect success in verifying client contributions while mitigating the risks of malicious watermark use. Additionally, it reduces GPU memory consumption by 85% and cuts processing time by at least 5× compared to the baseline. Our code is open-sourced at <https://anonymous.4open.science/r/Sanitizer-5933>.

Index Terms—federated learning, ownership and contributions verification, backdoor-based watermarks

1. Introduction

Federated Learning (FL) [1] is on its way to becoming a standard for training deep learning models with data distributed across clients. As the training data and the resultant model are of high commercial value [2]–[7], protecting their intellectual property (IP) has become particularly important [8]. To this end, backdoor attacks can serve as a positive means to embed a unique watermark into the model for ownership verification. During model training, one could train the model to recognize a special pattern known as a trigger, such that when the trigger is attached to the input, the model returns a predefined output regardless of the actual content [9], [10]. The special

This work was completed as a research assistant at HKU.

**Corresponding author*

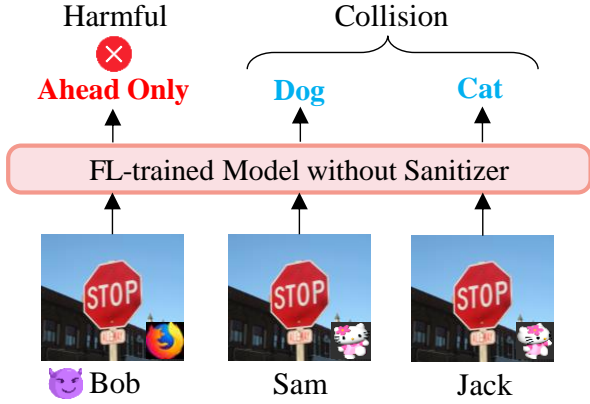


Figure 1: Without Sanitizer, a malicious client (e.g., Bob) can control the model by predicting a stop sign attached with a special trigger (originally used as a watermark) to be the “Ahead Only”. Watermark collision may also occur when two clients (e.g., Sam and Jack) use a similar trigger but designate different target labels.

pattern is often kept secret; hence, the demonstration of such non-intuitive behavior can be used as a watermark to claim the ownership or contributions.

This paper focuses on a common application scenario where FL clients co-own the jointly trained model [9], [11]–[15]. To achieve client-side contribution demonstrations, each client can simply embed a backdoor of their choice as a watermark. However, such an approach suffers from two problems (Figure 1).

- **Potential Misuse for Malicious Purposes:** Malicious clients can exploit watermarks to control model predictions in harmful ways [16]–[18], such as predicting a stop sign attached with a special pattern originally used as a watermark to be “Ahead Only.”
- **Watermark Collisions:** As clients (benign or malicious) choose their own trigger-output pair as the watermark, a collision may occur when two clients use a similar pattern as the trigger but designate different outputs (i.e., class labels). Such a collision can lead to both watermarks being unlearnable.

Overall, the use of backdoor attacks for client-side watermarking not only poses a serious security threat to FL but may also become an obstacle to IP protection in FL.

To alleviate the above problems, we explore a server-side sanitization process called Sanitizer, with an overarching idea of making all the implanted backdoors, whether

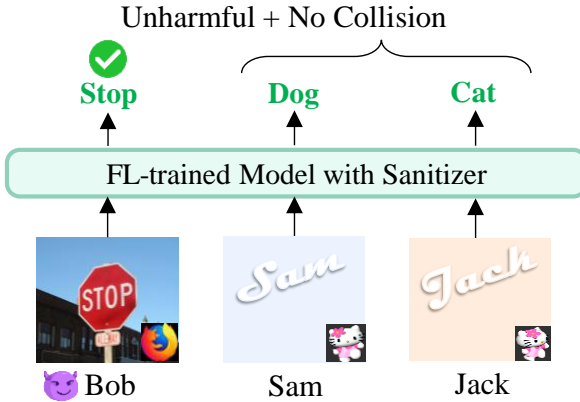


Figure 2: Sanitizer makes the trigger ineffective when placed on a natural image (e.g., Bob). But it enables trigger to output the target label as a watermark for IP protection only when placed in the client-specific unharmful environment (e.g., Sam and Jack), and no collision even if they use a similar trigger with different target labels.

they are benign or malicious, effective only in an unharmful environment. Sanitizer defines a client-dependent input subspace composed of unnatural samples and moves the backdoors implanted by each client to its designated subspace. As a server-side method, clients do not need to actively participate in Sanitizer and can embed watermarks as usual. As shown in Figure 2, Sanitizer makes the trigger ineffective when placed on a normal image, but it activates the backdoor and outputs a predefined target class when placed in the client-specific unharmful environment (i.e., a unique-color unnatural picture for this example) while mitigating potential backdoor conflicts among clients.

Challenges. A straightforward approach involves reverse engineering the hidden triggers embedded inside each client-submitted model at each round, unlearning them, and re-establishing the trigger-output associations in an unharmful environment post-FL. However, referred to as the baseline method in this paper, it is inefficient as reverse engineering at each round incurs significant resource and time consumption, making it impractical for FL applications, as shown in Figure 3 (red). To optimize the efficiency for FL, we need to minimize server-side processing time in each round to prevent delay in subsequent rounds during FL training, and we also need to ensure a low resource consumption to enable parallel trigger recovery across multiple client-submitted models.

In this paper, Sanitizer aims to efficiently sanitize backdoors for unharmful client-side watermarking. To tackle the challenges mentioned above, we propose to first extract a small backdoor subnet from each client-submitted model for reverse engineering, driven by the observation that backdoors are often encapsulated in a subset of neurons. Then, we take advantage of the iterative learning paradigm in FL and propose a lightweight method to recover the trigger implanted in each client-submitted model by spreading the reverse optimization across communication rounds. The trigger and target class gradually emerge and take shape over time. Based on the above two improvements, Sanitizer is efficient, requires minimal GPU resources, and does not hamper the

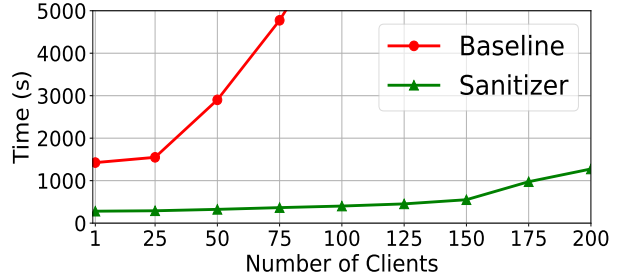


Figure 3: Sanitizer offers a significantly better scalability. It keeps the total server-side time consumption to run a 10-round FL on CIFAR10 with ResNet18 consistently lower (green) than the baseline (red) as the number of participating clients increases.

overall FL training process [19]. As shown in Figure 3, Sanitizer maintains consistently low time consumption (green). With only 25 clients, the baseline (red) takes approximately five times longer than Sanitizer. Given the fixed GPU memory of the server, the disparity between the two methods becomes more pronounced as the number of clients increases. Due to lower memory consumption, Sanitizer enables the server to process more client-submitted models in parallel. After completing the FL training, we employ an unharmful relearning process to “unbind” the trigger from the clean images and re-establish its association with the unique, unharmful environment of each client. Since each client-submitted model is processed independently before aggregation at each round and each client’s trigger is ultimately confined to its own unharmful client-specific input subspace, watermark conflicts will not arise during the verification phase. In summary, our key contributions are as follows:

- We introduce a server-side sanitization process that mitigates potential harmful use in backdoor-based client-side watermarking by enabling the triggering of counter-intuitive model behavior in unharmful environments.
- We investigate watermark collisions and propose a conflict resolution method by assigning each client a dedicated input subspace for contribution demonstration. Clients who coincidentally use similar triggers can still verify their contributions.
- We develop an efficient mechanism that leverages FL’s multi-round nature by spreading the reverse optimization of backdoors across communication rounds. This significantly reduces computational overhead, GPU memory usage, and processing time in each round, enabling Sanitizer to scale effectively in FL environments with a large number of clients.

We have conducted extensive experiments to verify Sanitizer’s broad applicability to different datasets and neural architectures. It achieves near-perfect success in verifying client contribution, eliminates the risks of malicious watermark use, and remains scalable.

2. Related Work

With AI Trust emerging as a critical industry concern, as noted in Gartner’s latest technology report [20], protecting IP in both centralized and FL-trained model remains a

significant ongoing research focus driven by the increasing commercial and legal demands [8], [21], [22].

Watermarking in Centralized Model. Many watermarking approaches have been proposed to protect the IP of DNN model. Broadly speaking, these methods can be categorized into two classes: the feature-based [23]–[27], requiring manipulating the loss function and model parameters, and the backdoor-based [28]–[32], involving injecting a trigger set with predefined output (known only to the model owner) as the watermark. Basically, these strategies for centralized DNN models lay the groundwork for the development of watermarking in FL, where the process is more complex due to the client-server learning protocol and specific privacy requirements [13], [33], [34].

Watermarking in FL-trained Model. Watermarking methods in FL can be generally categorized into server-side [17], [34] and client-side schemes, owing to the collaborative nature of client-server workflow [13]. We emphatically investigate the current client-side solutions of watermarking for IP protection in FL. One of the representative methods is FedIPR [9], which permits each client to embed their own backdoor-based and feature-based watermark into the model for contribution demonstration without exposing either their private watermark or training data to other clients. FedSOV [35] presents a cryptographic signature-based approach on top of FedIPR, allowing numerous clients to verify the ownership credentials through unforgeable digital signatures. FedCIP [33] is a feature-based watermarking framework that allows for traitor tracking while maintaining compatibility with FL security aggregation such as parameter encryption [36]. Merkle-Sign [37] are also used for client-side watermarking, which designs a security mechanism for distributed storage to protect both privacy and ownership. FedZKP [38] proposes a verification protocol based on the zero-knowledge proof for secure model ownership verification. Besides, [15] and [11] introduce a backdoor-based watermarking scheme for IP protection within a homomorphically encrypted FL framework using homomorphic encryption [36], [39] while preventing the watermarking updates from leakage.

Research Gap. However, we argue that existing client-side approaches have certain limitations that warrant consideration to ensure comprehensive IP protection in FL. First, malicious clients can embed harmful misclassification rule as a malicious backdoor into the model under the guise of backdoor-based [16] watermarking, thereby compromising the model integrity and posing a significant security threat [17], [18] to real-world applications. Second, similar backdoor trigger pattern with different target labels of any two clients is likely to cause collisions, resulting in both watermarks becoming unlearnable [14], [40]. In contrast, to address these limitations, Sanitizer provides a client-agnostic server-side sanitization pipeline, not only makes the client-side watermarks unharmed but also resolves conflicts when different clients use a similar trigger with different target labels as the watermark.

3. Preliminaries

Backdoors can evidently be utilized for both benign and malicious purposes. In this paper, when distinguishing between different purposes, we use the term “watermark”

for backdoors serving benign purposes such as IP protection, and the term “harmful backdoor” or “malicious backdoor” for those serving malicious ones such as model control. Fundamentally, both purposes represent the same technique—a specific trigger-output pair embedded into a model. We use the term “backdoor” when uniformly referring to the backdoor itself without specifying purposes. These terms are used consistently throughout the paper.

In this section, we give the threat model (Section 3.1), clarify the capabilities (Section 3.2) and goals (Section 3.3) of Sanitizer, and define the poisoning formulation and unharmed setting in our context (Section 3.4).

3.1. Threat Model

We consider the threat model, where adversaries from malicious clients may launch the harmful backdoors instead of watermarks during the watermark embedding phase. In our setting, clients are authorized to embed legitimate backdoor-based watermarks into models as proof of co-ownership or contribution during the local training phase. However, adversaries on malicious clients may exploit this privilege to unlawfully implant harmful backdoor rather than watermark, and finally, control the model during inference phase for harmful purposes. It is straightforward and accessible to every client, simply placing a trigger pattern on normal data and designating a harmful target label, in line with [16], [28], [41]. Thus, the security of backdoor-based client-side watermarking is not guaranteed. Additionally, all clients do not cooperate with the server-side sanitization process.

3.2. Capabilities of Sanitizer

Consistent with prior works [1], [17], [34], [42], the server is considered a trusted and honest party employed by the collaborating clients to facilitate FL. Sanitizer runs on the server-side and has access to the compromised models received from clients. However, it cannot interfere with the standard local training process, modify client-side operations, or access the full local dataset of individual clients. Moreover, Sanitizer has no prior knowledge about the potential backdoor triggers or target classes, and does not distinguish between benign and harmful backdoors. Similar to most existing defenses [43]–[48], Sanitizer can only get access to a limited small portion of reserved clean dataset as defense data, which is common and only designed to drive the sanitization mechanisms. We exclude the defense data from all clients’ local training dataset, demonstrating that there is no overlap between them.

3.3. Goals of Sanitizer

Sanitizer intends to achieve the following objectives, each of which plays a crucial role in safeguarding IP in FL:

- **Effectiveness.** Effectiveness implies that Sanitizer makes each client deterministically demonstrate their co-ownership or contribution to the FL-trained model by achieving near-perfect success in verifying the watermark in their respective unharmed environment, while ensuring no conflicts arise among them.

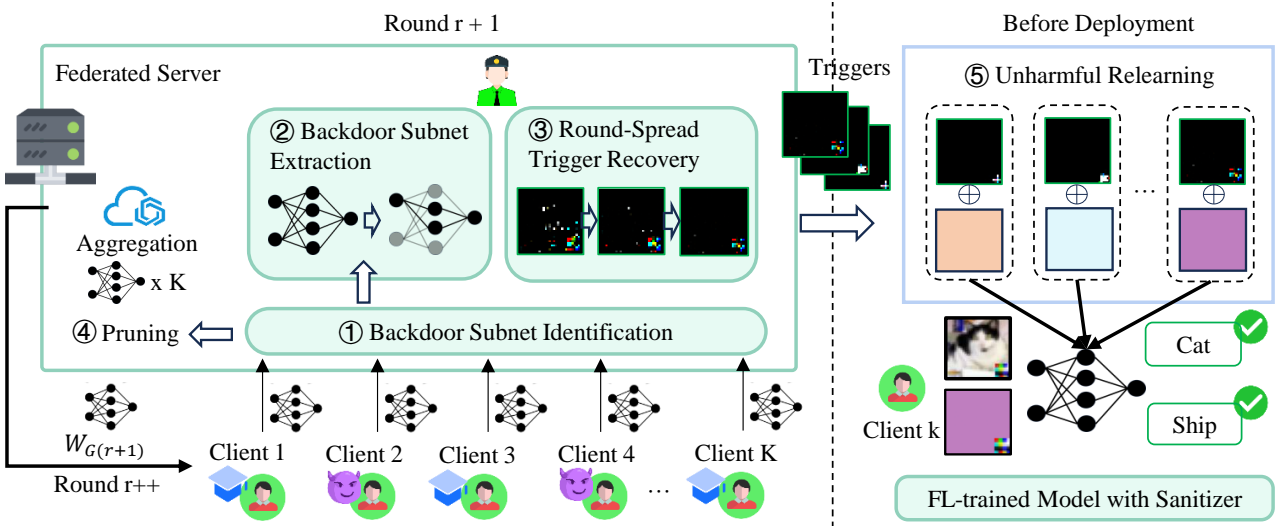


Figure 4: Overview of Sanitizer pipeline. Sanitizer introduces three key enhancements on the server-side during the FL process: ① Backdoor Subnet Identification and ② Extraction, ③ Round-spread Trigger Recovery, and ④ Pruning and Aggregation for the next round. After the FL process, ⑤ Unharmful Relearning ensures that the resultant FL-trained model is embedded with unharmful watermarks, making it ready for deployment.



Figure 5: Examples of harmful (natural) inputs compared to the unharmful (artificial) inputs of each client (e.g., Bob, Sam, and Jack).

- **Harmlessness.** Harmlessness means that Sanitizer removes the malicious backdoor effects from the FL-trained model, preventing backdoors from being triggered on natural queries during the inference phase.
- **Fidelity.** Fidelity refers to the requirement that Sanitizer should have negligible impact on the main functionality and integrity of the FL-trained model, maintaining high accuracy on clean test samples.
- **Efficiency.** The sanitization process should run in an efficient manner during the FL process, characterized by the low time and resource consumption on the server-side, two crucial factors in this context.

3.4. Notations

Poisoning Formulation. Given a client k , training a backdoored model can be formulated as a multi-objective

optimization problem, with the following objectives:

$$\min_{\theta_k} \mathbb{E}_{(\mathbf{x}_c, y_c) \in \mathcal{D}_c} \mathcal{L}(f(\mathbf{x}_c; \theta_k), y_c) + \mathbb{E}_{(\mathbf{x}_t, y_t) \in \mathcal{D}_t} \mathcal{L}(f(\mathbf{x}_t; \theta_k), y_t), \quad (1)$$

in which \mathcal{D}_c is the clean dataset of client k , and \mathcal{D}_t is its trigger set for benign or malicious purposes. Besides, f denotes the standard classifier parameterized by θ_k . \mathcal{L} denotes a standard loss function, e.g., cross-entropy.

Unharmful Setting. We consider the unharmful dataset \mathcal{D}_u as a collection of unnatural images that lack practical significance and have no impact on the main task of the FL-trained model. Note that \mathcal{X}_u must satisfy $\mathcal{X}_u \cap \mathcal{X}_c = \emptyset$, where \mathcal{X}_u denotes the artificial input subspace and \mathcal{X}_c denotes the clean input space, indicating no overlap between them, and ensuring \mathcal{X}_u is distinct and significantly distant from the main task. In our setting, all the watermarks and backdoors should be transformed into an unharmful environment (i.e., being treated equally), which is artificially and uniquely tailored for each client. For example, as shown in Figure 5, we use a set of distinct and unnatural inputs in unique colors as the unharmful environments, compared to the harmful (natural) inputs.

4. Methodology

4.1. Overview

As illustrated in Figure 4, we put forth the following Sanitizer pipeline, a protection mechanism on the server-side, which is implemented with a suite of techniques aimed at safeguarding the backdoor-based client-side watermarking process in FL. During each round, Sanitizer does not interfere with the client-side standard training procedure where clients embed backdoors as usual. Upon receiving the client-submitted models, the corresponding sanitization actions are initiated.

Outline. Sanitizer is accomplished by three procedures during FL process: first, we identify and extract the backdoor subnet (Section 4.2 and Section 4.3), followed by an efficient inversion of the backdoor trigger (Section 4.4), and simultaneously perform pruning and aggregation (Section 4.5) after the identification of backdoor subnet. After completing the FL process, we conduct a final step of unharmed relearning (Section 4.6) to achieve the final unharmed effectiveness of Sanitizer. We present the details in the following sections, exemplified using a specific client k at a certain round $r + 1$; the approach remains consistent and independent across all clients.

4.2. Backdoor Subnet Identification

As previously mentioned, performing a standard reverse engineering (such as a complete process following Neural Cleanse [49]) on each client-submitted model at the server-side is of high resource and time consumption [43], [45], [50], [51]. *Can we reduce the server’s load and accelerate the whole sanitization process during the FL?* Our answer is affirmative and the detailed steps before aggregation in each round work as follows:

First, we develop an intuition that we can leverage a small backdoor subnet stemming from the entire client-submitted model to replace the whole one for reverse engineering. Given the architecture of the target model, its backdoor subnet has the same layer type and structure to that of the entire network, but each layer only contains few backdoor-related neurons or channels. This results in a smaller network with the same architecture while largely preserving the backdoor functionality, and the subnet is strongly sensitive to backdoor trigger only. We derive this key insight from the fundamental properties of a backdoored model: the existence of a backdoor subnet within it, dominating backdoor functionality (i.e., exhibiting a high backdoor accuracy), consistent with the essential arguments presented in [16], [45], [52]–[55]. The high-level idea is that the backdoor task (i.e., learning the trigger features) is often much “easier” than the benign task (i.e., learning the semantic or natural features), existing a high level of independence between the two tasks. Consistent with [56], we denote $f_s(\theta_k^*)$ as the identified backdoor subnet of the client-submitted model $f(\theta_k)$, which needs to satisfy the following conditions:

- The network architecture of subset $f_s(\theta_k^*)$ must be structurally consistent with $f(\theta_k)$, ensuring alignment in the number of both input and output dimensions.
- The number of parameters of $f_s(\theta_k^*)$ should be strictly less than that of $f(\theta_k)$, i.e., $|\theta_k^*| < |\theta_k|$.
- The difference in activation value of each neuron within the backdoor subnet $f_s(\theta_k^*)$ when processing a clean sample x_c versus a backdoor sample x_t should be significant. A neuron’s activation value refers to the output value of the neuron during forward propagation. Specifically, this implies that each neuron within backdoor subnet $f_s(\theta_k^*)$ fires large activation value, denoted as a_t , when the backdoor input x_t is provided, while remaining inactive with a small activation value, denoted as a_c , on the clean input x_c , i.e., $|a_t - a_c| \gg 0$.

Second, to identify the small backdoor subnet, which is composed of backdoor-related units, we perform clean unlearning and introduce the Unit Weight Changes (UWC)

to quantify the backdoor relevance (importance) of each unit in the backdoored model. This is based on an empirical observation: during the clean unlearning process, the weights of backdoor-related units undergo significant changes. Hence, a larger UWC value for a specific unit signifies a stronger association with the backdoor behavior. Specifically, given a client-submitted model $f(\theta_k)$ parameterized by θ_k uploaded from client k and (x_d, y_d) from defense data D_d , clean unlearning can be described as the inverse procedure of model training, achieved by maximizing its loss on the given data D_d . The maximization problem towards $f(\theta_k)$ consistent with [57] is formulated as follows:

$$\max_{\theta_k} \mathbb{E}_{(x_d, y_d) \in D_d} \mathcal{L}(f(\mathbf{x}_d; \theta_k), y_d). \quad (2)$$

Note that, this step easily removes the main functionality by making clean accuracy close to a random guess level quickly. The resulting unlearned network $f(\theta'_k)$ exhibits high backdoor activations, indicating that the backdoor functionality has been preserved [58], [59]. Then, we put forward the definition of UWC for unit $o \in \{1, \dots, O_\ell\}$ in layer $\ell \in \{1, \dots, L\}$ formally, as follows:

$$\text{UWC}_{\ell, o} = \sum_{i=1}^{\text{Dim}} \left| \theta_{\ell, o, i}^{\text{post}} - \theta_{\ell, o, i}^{\text{pre}} \right|, \quad (3)$$

where θ^{pre} and θ^{post} are the weight matrix before and after clean unlearning, respectively, and $\sum |\cdot|$ denotes the sum of absolute differences over all relevant statistical dimensions, also named $L1$ norm. Dim refers to the aggregation dimension when calculating UWC. The granularity (neuron or channel) at which units are defined depends on the specific network architecture used in the layer, leading to variations in the specific representation of UWC. We focus primarily on two fundamental architectures in our paper. Specifically, for fully connected (FC) layer, we consider each neuron as a unit, and the statistical dimension Dim of each neuron is its sub-weights between adjacent layers. For convolutional (Conv) layer, calculations are performed at the channel level, summing over the I , H , and W dimensions, which denotes the total number of input channels, kernel height, and kernel width, respectively. They are the statistical dimension Dim of the Conv layer. Besides, we can control the size of the constructed backdoor subnet by selecting the backdoor units corresponding to topN% UWC from the sorted order in each layer. We will show the impact of different backdoor subnet sizes on Sanitizer in Section 5.7.

4.3. Backdoor Subnet Extraction

Following preliminary procedure, the backdoor subnet is identified by comparing differences in units’ weight maps, dispensing with the need to rely on previous methods [16], [49] that observe activation values based on pre-known trigger inputs. To achieve the efficiency in FL, Sanitizer aims to extract and leverage the identified small backdoor subnet for trigger recovery. We put forward the steps of backdoor subnet extraction.

After identifying the backdoor subnet $f_s(\theta_k^*)$, we design a subnet-extraction algorithm to extract it from the client-submitted model $f(\theta_k)$. The algorithms vary

depending on the architectures. As the extraction algorithms differ, leading to varying levels of implementation complexity. While similar to pruning [60], [61], it is not identical. We give the high-level description of subnet-extraction algorithm below:

- Construct an automatically initialized “narrow” network f_i with the same architecture as $f(\theta_k)$ (including the number of both input and output dimensions) based on the size of the envisioned backdoor subnet.
- Copy the corresponding weights w and bias b of the selected backdoor units from $f(\theta_k)$ to f_i serving as $f_s(\theta_k^*)$, according to the indices in the sorted order UWC list of the backdoor units in each layer.

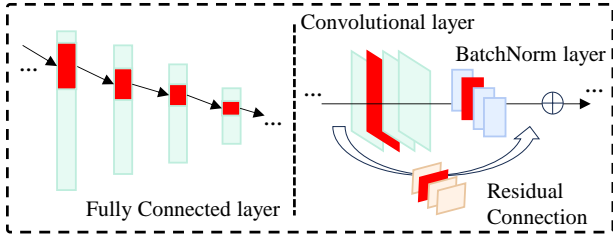


Figure 6: Two types of backdoor subnets (red) responsible for producing the predefined output. The left panel presents the FC-type backdoor subnet, while the right depicts the Conv-type backdoor subnet with BN-layer.

As shown in Figure 6, for FC layers (left), only the sub-weights $w_{v_1 v_2}$ between the selected backdoor neurons of the preceding layer and following layer are retained, where v_1 and v_2 represent the sets of selected neurons in adjacent layers. In contrast, all other connections’ sub-weights $w_{\tilde{v}_1 v_2}$, $w_{v_1 \tilde{v}_2}$, and $w_{\tilde{v}_1 \tilde{v}_2}$ connecting two layers are discarded, where \tilde{v}_1 and \tilde{v}_2 denote the sets of unselected neurons in the corresponding layers. For Conv layers (right), the consistency between the number of channels in the preceding and following layers must be maintained. Additionally, the channels in the subsequent BatchNorm layer that correspond to the selected channels in the preceding Conv layer should be preserved. Particular attention should be given to residual connection, ensuring that the selected channels in both the main and residual connection are identical. We also consider Depthwise and Pointwise convolutions, which are two specialized Conv layers commonly employed in the lightweight architectures, such as MobileNet. Detailed implementation is provided in the source code. Generally, the extracted backdoor subnet is yet another neural network model, which is used for round-spread trigger recovery.

4.4. Round-spread Trigger Recovery

To further reduce the time consumption, we propose conducting round-spread trigger recovery on the extracted small backdoor subnet, taking advantage of the multi-round iterative learning inherent in FL. Specifically, instead of conducting a full reverse engineering process in each round, we distribute the iterations of the full reverse engineering across multiple communication rounds, meaning that the entire reverse engineering process is completed progressively once throughout the entire FL period. In this design, we leverage information from previous

rounds, such as the results of reverse engineering from the last round for each client. Formally, for client k , we follow the general optimization problem [49], but apply it specifically to the subnet $f_s(\theta_k^*)$, as outlined:

$$\min_{\mathbf{m}, \Delta} \mathcal{L}(f_s(x'_d; \theta_k^*), y_t) + \lambda \cdot |m|, \quad (4)$$

where $x'_d = (1 - m) \cdot x_d + m \cdot \Delta$, $x_d \in D_d$. Variables m and Δ mean the mask and trigger pattern. We employ a dictionary structure to track masks and trigger patterns. In this way, Sanitizer allows the trigger pattern to emerge incrementally with partial recovery in each communication round, with the target class being detected via outlier detection [49] at the end. This approach significantly reduces the time cost on the server-side while ensuring that the backdoor trigger is effectively reconstructed over time during the FL process.

Following the processes mentioned, the parameters size and network complexity of the model for reverse engineering are significantly reduced, along with a notable reduction in GPU memory utilization. Additionally, the optimization iterations, i.e., the epochs for reverse engineering, are evenly distributed across communication rounds in FL. As a result, the total time required for sanitization actions in each round will be reduced, enabling server to handle more client-submitted models in parallel, without delaying the progress of the next communication round during the FL process. We will present the experimental results in Section 5.

4.5. Pruning and Aggregation

Similarly, after identifying the backdoor subnet, we simultaneously perform pruning on the $f(\theta_k)$ by setting the parameters correspond to the backdoor units to zero without reducing the number of parameters, effectively removing the backdoor effect and obtaining a new network $f(\tilde{\theta}_k)$ with parameters matrix $\tilde{\theta}_k$. The pruning rate is consistent with the size of the identified backdoor subnet, as described in Section 4.2. The aggregation conducted on θ_k , $k \in \{1, \dots, K\}$ at $t + 1$ round is as follows:

$$\theta_{global}^{t+1} = \sum_{k=1}^K \frac{n_{(k)}}{n} \tilde{\theta}_k^{t+1}, \quad (5)$$

where $n_{(k)}$ denotes the number of data samples locally held by client k , and n represents the total number of data samples locally held by the K clients: $n = \sum_{k=1}^K n_{(k)}$. The entire multi-round FL process with Sanitizer will follow the aforementioned procedures until it converges.

4.6. Unharmful Relearning

As the FL training is completed, the reversed trigger pattern Δ and target class y_t for each client are also obtained. Following the basic structure of finetuning [62], [63], we construct an unharmful artificial dataset \mathcal{D}_u and put the pattern Δ on the unharmful image $x_u \in \mathcal{D}_u$ to retrain the FL-trained model $f(\theta)$ in order to re-establish the watermark’s mapping from input to output. For each client k , the watermark would satisfy the below mapping:

$$f(x_u^k + \Delta^k) \rightarrow y_t^k, \quad (6)$$

Table 1: WDR, ASR, and ACC of Sanitizer compared to the without-Sanitizer under the non-conflicting scenarios across different datasets. Sanitizer maintains an exceptional WDR after sanitization and reduces the ASR to a level comparable to random guessing. The vanilla ACCs without any embedded backdoors or sanitization process are also reported.

Task	Method	vanilla ACC	Scenario without Backdoor Conflicts		
			WDR↑	ASR↓	ACC↑
FMNIST	without-Sanitizer	90.02%	100.00%	98.95%	84.13% (↓ 5.89%)
	Sanitizer		99.20%	13.84% (↓ 85.11%)	87.20% (↓ 2.82%)
CIFAR10	without-Sanitizer	92.12%	98.88%	97.01%	88.06% (↓ 4.06%)
	Sanitizer		99.95%	12.22% (↓ 84.79%)	87.18% (↓ 4.94%)
TinyImageNet	without-Sanitizer	56.61%	97.02%	97.89%	52.20% (↓ 4.41%)
	Sanitizer		100.00%	1.55% (↓ 96.34%)	51.08% (↓ 5.53%)

which leads to a new unharful watermark effect (i.e., producing predefined target class y_t^k when trigger is applied to the unique x_u^k). The minimization problem of unharful relearning towards $f(\theta)$ is formulated as follows:

$$\min_{\theta} \alpha \cdot \mathbb{E}_{(\mathbf{x}_d, y_d) \in \mathcal{D}_d} \mathcal{L}(f(\mathbf{x}_d; \theta), y_d) + \beta \cdot \mathbb{E}_{x_u^k \in \mathcal{D}_u} \mathcal{L}(f(x_u^k + \Delta_t^k; \theta), y_t^k), \quad (7)$$

where α and β are the loss weight to balance the two loss contributions. Each client’s trigger is confined to its own harmless, client-specific input subspace. This targeted confinement makes watermarks only work in their own unharful environment, preventing them from ambiguous contribution claims. After relearning, we achieve the unharful, watermarked FL-trained model, which serves as a valuable product with commercial or legal properties.

4.7. Contribution Verification

After sanitization, the unharful, watermarked FL-trained model is ready for deployment, and all clients will be told their own unique x_u , which can be regard as a kind of key or certificate. Only with the key will the trigger present its pre-designed effect, serving as a watermark for contribution demonstration. Additionally, clean inputs will be classified into the ground-truth class, even if they are stamped with a trigger. We follow the verification procedures of existing key works in this field [9], [11], [17]. In the inference phase, when a client attempts to verify its contribution, it can access the model via an API in black-box mode, check the feedback, and calculate watermark accuracy based on (6). If the watermark accuracy is higher than a present threshold σ (e.g., 95%), the contribution is successfully verified. The unharful environment x_u of each client is proprietary and confidential information, which should be kept secret and not disclosed to other clients.

5. Performance Evaluation

In this section, we present our experimental evaluation of the proposed Sanitizer in terms of effectiveness, harmlessness, fidelity, and efficiency.

5.1. Experimental Setup

Datasets and Models. We train the FL system following our Sanitizer pipeline on three widely studied benchmark datasets: Fashion-MNIST (FMNIST) [64], CIFAR10 [65], and TinyImageNet [66] using a diverse set of well-known architectures for image classification tasks: a 5-layer MLP for FMNIST, a ResNet18 [67] and MobileNetV3 [68] for both CIFAR10 and TinyImageNet. CIFAR10 with ResNet18 serves as the default dataset and architecture.

Evaluation Metrics. We report our evaluation results in terms of two metric categories: effectiveness and efficiency. Specifically, the watermark detection rate (WDR) [9], [13], expressed as a percentage, measures the likelihood that trigger patterns in unharful environments are classified into the target class. Clean accuracy (ACC) assesses the performance of the main task, commonly referred to as fidelity. To assess harmlessness, we report attack success rate (ASR) of the final FL-trained model after sanitization. As for efficiency, we evaluate Sanitizer’s resource and time consumption by considering the GPU memory utilization (GPU_Mem) and runtime cost (Time).

Configuration and Hyperparameters. Following the basic setup of existing works [9], [17], [34], [60], [69], by default, we utilize FedAvg [1] as the aggregation backbone, and simulate $K = 20$ participating clients, with half are malicious (embedding a malicious backdoor), while the other half are benign (embedding a benign watermark) for aggregation. Different values of K are also provided for evaluating scalability. The number of communication rounds is set to 100. We employ stochastic gradient descent (SGD) optimization with $E = 5$ local epochs, a local initial learning rate of $lr = 0.01$, and a batch size of 128. The default poisoning rate for each client per round is fixed at 10%. We specify that the default backdoor subnet size rate is set to 20%. The rate of defense data is 0.05 of the whole dataset and reverse engineering epochs is 2 for each round. We establish a unique pixel pattern of different shapes as the backdoor trigger pattern for each client and allocate a background image with a distinct solid color as the unharful environment. To ensure the rigor of the evaluation, all major experiments are conducted

Table 2: WDR, ASR, and ACC of Sanitizer compared to the without-Sanitizer under the conflicting scenarios across different datasets. Sanitizer maintains an exceptional WDR after sanitization and reduces the ASR to a level comparable to random guessing. The vanilla ACCs without any embedded backdoors or sanitization process are also reported.

Task	Method	vanilla ACC	Scenario with Backdoor Conflicts		
			WDR↑	ASR↓	ACC↑
FMNIST	without-Sanitizer	90.02%	49.31%	97.83%	88.06% (↓ 1.96%)
	Sanitizer		100.00%	11.21% (↓ 86.62%)	86.98% (↓ 3.04%)
CIFAR10	without-Sanitizer	92.12%	62.30%	98.23%	87.50% (↓ 4.62%)
	Sanitizer		99.75%	10.55% (↓ 87.68%)	86.92% (↓ 5.20%)
TinyImageNet	without-Sanitizer	56.61%	67.85%	95.44%	51.58% (↓ 5.03%)
	Sanitizer		98.71%	3.02% (↓ 92.42%)	50.16% (↓ 6.45%)

independently in triplicate, and we report the average value. We implement Sanitizer using PyTorch-2.4 and run all experiments on a server with an AMD EPYC 7542 CPU (32 cores), 512 GB of memory, and an NVIDIA V100S GPU (32 GB), running Ubuntu 20.04 LTS on the CloudLab platform [70].

Outline. We first evaluate the effectiveness of the proposed method Sanitizer compared to the without-Sanitizer in Section 5.2 and Section 5.3. Then we illustrate the performance of trigger recovery for certain clients across conflicting and non-conflicting scenarios (Section 5.4). In Section 5.5, we analyze the efficiency of Sanitizer against the baseline and further explore the scalability of Sanitizer. We show Sanitizer is applicable across different neural architectures in Section 5.6. Finally, we show Sanitizer’s effectiveness and efficiency under different variants in Section 5.7.

5.2. Effectiveness in Non-conflicting Scenario

We first evaluate Sanitizer compared to without-Sanitizer (i.e., existing backdoor-based client-side watermarked FL without Sanitizer) in terms of watermark effectiveness (WDR), harmfulness (ASR), and fidelity (ACC) under the non-conflicting scenario we set. Table 1 reports the average results obtained from evaluating the final FL-trained model. Besides, a vanilla ACC of an FL-trained model without any embedded backdoors or sanitization process is also provided as a reference for comparisons.

On one hand, it can be observed that the WDR, averaged across all benign clients, of the model without Sanitizer is high, all exceeding 97%, while the ASR, averaged across all malicious clients, also exhibits a substantial level of at least 97% for all datasets. Both watermarks and harmful backdoors remain active in the unprotected watermarked FL-trained model. These results indicate that malicious clients can effortlessly implant malicious backdoors into the model for harmful purposes during the backdoor-based client-side watermarking process, underscoring the inherent vulnerability and susceptibility of the FL-trained model in this context.

In contrast, after applying Sanitizer to FL, the WDR consistently remains at least 99% across three datasets, which is high enough for ownership and contribution

verification. Furthermore, the ASR is dramatically reduced to a random guess level, with a sharp drop compared to without-Sanitizer. In particular, the ASR for all three tasks demonstrates a reduction of over 84%. Sanitizer causes a slight decrease in the model’s ACC compared to the vanilla ACC, similar to the behavior observed in without-Sanitizer. Taken together, these results reveal several outcomes achieved by Sanitizer. First, Sanitizer successfully transforms the watermarks into an unharful state, thus confirming the effectiveness of our novel unharful watermarks in FL. Simultaneously, Sanitizer effectively mitigates the threats of malicious backdoors, demonstrating its ability to precisely identify and prune the backdoor subnets from the client-submitted models. Specifically, this prevents backdoors from being triggered in natural queries, thus safeguarding the model’s integrity. Furthermore, Sanitizer has a negligible impact on the fidelity of the FL-trained model. Although there is a slight drop in ACC hovering around 5%, the trade-off is acceptable in our context in light of the substantial reduction in ASR.

Collectively, Sanitizer offers strong effectiveness in making watermarks unharful in FL, and is widely applicable and not restricted to specific datasets.

5.3. Effectiveness in Conflicting Scenario

In the scenario with backdoor conflicts, we introduce multiple pairs of watermark conflicts among the benign clients. Specifically, we design the same trigger targeting different labels, thereby creating deliberate conflicts in watermark verification. As presented in Table 2, without-Sanitizer is unable to achieve a satisfactory WDR, while the corresponding ASR remains dangerously high. This confirms that conflicts compromise the effectiveness of the watermark by making them being unlearnable, leading to ambiguous contribution claims. Meanwhile, the backdoor attack remains highly effective. After Sanitizer conducts the unharful transformation for every backdoor independently, the WDR improves to an impressive rate exceeding 98%, which is sufficient for contribution verification. More importantly, the ASR experiences a marked reduction of at least 86% and ACC also remains competitive at a considerable level, with a moderate ACC drop of around 5% induced by Sanitizer. The experimental results across

Table 3: Two sets of visual original trigger pattern examples and their recovered versions by Sanitizer from CIFAR10 in the scenarios of non-conflicting and conflicting. In all cases, the corresponding trigger is successfully recovered, and each is assigned a unique input subspace as the unharful environment. This targeted assignment ensures that a high WDR is achieved only within its respective unharful environment.

(a) Scenario without trigger-output conflicts between clients.

Client (Target Class)	Trigger	Reversed Trigger	Unharful Environment	WDR
Client 1 (1)				100.00%
Client 5 (2)				99.96%
Client 9 (3)				99.28%

(b) Scenario with trigger-output conflicts (e.g., Client 1 and 5).

Client (Target Class)	Trigger	Reversed Trigger	Unharful Environment	WDR
Client 1 (1)				99.98%
Client 5 (2)				99.93%
Client 9 (3)				98.69%

three datasets are consistent with those observed in the non-conflicting setting. Sanitizer reduces the ASR to a near-random guess level while maintaining a high WDR and a robust ACC in the conflicting scenario. What stands out from this experiment is that Sanitizer also effectively transforms the conflicting backdoors into unharful and conflict-free ones, while mitigating the harmful backdoor effect and preserving the main functionality in scenario with backdoor conflicts.

To distill the findings, Sanitizer consistently demonstrates its general effectiveness in both conflict-free and conflict-present scenarios. Why is it effective? The key lies in its ability to successfully and systematically reverse the embedded trigger pattern in each client-submitted model during the FL process, and eventually confine them to their own unharful, client-specific subspace. We will provide a more in-depth explanation via visualization in the following subsection.

5.4. Visual Examples of Trigger Inversion

The previous results demonstrate the overall effectiveness of Sanitizer. In this subsection, we focus on specific clients and employ trigger visualization to further validate the effectiveness of Sanitizer in trigger pattern recovery. All hyperparameters and configurations are maintained at default settings. Table 3 provides two visual example sets of the original trigger patterns (2nd column) and their eventually recovered versions (3rd column) by Sanitizer from CIFAR10. In the scenario without trigger-output conflicts (Table 3a), we apply three distinct, commonly used patch-like patterns to the clean data for three participating clients (Client 1, Client 5, and Client 9), setting their desired outputs to different classes (1, 2, and 3) respectively. As we can see, in all cases, the corresponding backdoor trigger is successfully recovered, regardless of whether its real-world purpose is benign or malicious. Specifically, Client 1 achieves a notable trigger recovery

and reached a WDR of 100.00% after Sanitizer relearns the reversed trigger-output mapping rule into the unique and unharful input subspace (4th column). Client 5 and Client 9 demonstrate comparable recovery performance with WDR of 99.96% and 99.28%, respectively.

On the other hand, Table 3b presents results in the scenario where trigger-output conflicts exist, particularly between Client 1 and Client 5, both of whom use an identical trigger pattern (a white square block) while aiming for different target classes (label 1 and label 2). We observe that Sanitizer is insensitive to the presence of backdoor conflicts, as the trigger patterns recovered by Sanitizer continue to be feasible, and the WDR consistently remains high, with Client 1, Client 5, and Client 9 exhibiting 99.98%, 99.93%, and 98.69%, respectively. This effectiveness is attributed to two facts. First, each client is processed independently before aggregation during the FL process. Second, the final unharful input subspace is client-specific, effectively resolving the conflict issue. Furthermore, we observe that recovering the trigger from an FL-trained model without Sanitizer appears to be not feasible. Additional results can be found in the Appendix.

Analysis on Effectiveness of Trigger Inversion. First, why can the small extracted backdoor subnet stemming from the client-submitted model be used for trigger inversion? Thanks to the clean unlearning part (Section 4.2), we identify a small set of backdoor-related units within the original client-submitted model, which constitute a backdoor subnet. This backdoor subnet fully encapsulates backdoor knowledge while preserving most of the backdoor functionality, as demonstrated by the low ACC and high WDR of the subnet. For instance, on the CIFAR10 using ResNet18, the backdoor subnet achieves an average ACC of 14.60% and WDR of 99.98%. When applying the trigger recovery and backdoor detection on the extracted backdoor subnet, one can more easily expose the potential backdoor target and enhance the quality of the recovered trigger pattern. Second, why is the round-spread

Table 4: Efficiency comparison of the baseline and Sanitizer on CIFAR10 using ResNet18 and MobileNetV3. Sanitizer demonstrates significantly improved efficiency compared to the baseline on two architectures, with a substantial reduction in both resource and time consumption while maintaining comparable effectiveness to the baseline.

Method	CIFAR10 & ResNet18			CIFAR10 & MobileNetV3		
	GPU_Mem	Time	Precision			
Baseline	1322MB	142.50s	WDR:99.87% ASR:12.98% ACC:88.70%	273MB	84.88s	WDR:99.06% ASR:13.22% ACC:87.34%
Sanitizer	194MB (↓ 85.32%)	28.12s (↑ 5x)	WDR:99.95% ASR:12.22% ACC:87.18%	65MB (↓ 76.19%)	17.46s (↑ 4.8x)	WDR:100.00% ASR:9.75% ACC:84.66%

trigger recovery feasible? In each round, the models at the client-side are trained on a sanitized global model from the previous round, and they undergo continuous backdoor attacks for either benign or harmful purposes in this round. The backdoor task exhibits rapid convergence, achieving a high WDR or ASR greater than 99% quickly during local training. Upon receiving each client-submitted model, Sanitizer utilizes the results of reverse engineering from the previous round for that client as the initial values for the reverse optimization in the current round, ultimately facilitating the successful reconstruction of the backdoor trigger for each client. Moreover, a key aspect of Sanitizer’s effectiveness is that the trigger from each client is confined to its own harmless and client-specific input subspace (i.e., being effective only in the unharmed environment), which is directly attributed to the success of the trigger inversion step.

5.5. Efficiency and Scalability Studies

5.5.1. Efficiency of Sanitizer. As both Sanitizer and the baseline (described in Section 1) aim to achieve the identically expected effectiveness, we primarily evaluate the differences in their efficiency during the FL process, which is a critical concern in real-world FL applications. To this end, we evaluate the efficiency of the two methods on two different architectures, with the other settings kept identical to those in Section 5.3. We use the following primary metrics: (i) the GPU memory utilized GPU_Mem (MB) for processing one client-submitted model during server-side operations and (ii) the average runtime Time (seconds) of server-side operations per round during FL.

Results on ResNet18. Table 4 reports the results. What most strikingly emerges from it is that despite both approaches achieve considerable effectiveness, Sanitizer exhibits significantly less overhead in terms of resource consumption and runtime compared to the baseline. Specifically, the baseline consumes 1,322 MB of GPU memory for each client-submitted model, and takes 142.50 seconds for server-side execution per round. On the contrary, Sanitizer drastically reduces the GPU memory usage to 194 MB with an 85% reduction, which suggests that in each round, the server can process more client-submitted models in parallel. Moreover, the runtime optimization achieved by Sanitizer per round over the baseline is also particularly significant, with a 5x speedup in execution time from 142.50 to 28.12 seconds, highlighting the effi-

ciency gains provided by Sanitizer. With the significantly reduced resource and time consumption, Sanitizer still maintains non-trivial effectiveness, closely aligning with the performance of the baseline.

Results on MobileNetV3. The architectures in the MobileNet family are inherently designed with fewer parameters and lower computational cost compared to those in the ResNet family. As shown in Table 4, the experimental results consistently display similar behaviors. Remarkably, Sanitizer shows a drop of over 75% in GPU memory consumption and an approximately 5x speedup in runtime per round compared to the baseline. Meanwhile, as illustrated, Sanitizer also achieves the intended sanitization results. Together these results indicate Sanitizer’s suitability for lightweight neural architectures, which are commonly used in resource-constrained environments where computational and memory limitations are critical considerations.

In this subsection, we derive the important insight that Sanitizer demonstrates a significant efficiency advantage while maintaining comparable effectiveness, harmlessness, and fidelity. This is attributed to the fact that Sanitizer performs the round-spread trigger recovery on the extracted small backdoor subnet, two improvements introduced to accelerate the entire FL period. Moreover, the reduction in the GPU memory consumption makes Sanitizer particularly attractive for IP protection in resource-constrained FL environments. Interestingly, this may reflect the scalability of Sanitizer, as already shown in Figure 3 of Section 1, prompting us to further investigate this characteristic, which will be discussed in detail in the subsection 5.5.2.

5.5.2. Scalability of Sanitizer. To evaluate the scalability of Sanitizer, we examine the total server-side time consumption of two methods during the whole FL process as the number of participating clients increases over a 10-round FL on CIFAR10 using ResNet18. Figure 3 clearly showcases the scalability advantage of Sanitizer when compared to the baseline. Specifically, for the baseline, the time cost increases rapidly, showing near-exponential growth beyond 50 clients. Notably, with 75 clients, the baseline requires over 4,500 seconds to complete, which exceeds the acceptable range we set, and this steep upward trend persists as the number of clients continues to rise. Such scaling behavior suggests the baseline struggles to maintain practical efficiency in large-scale FL scenarios,

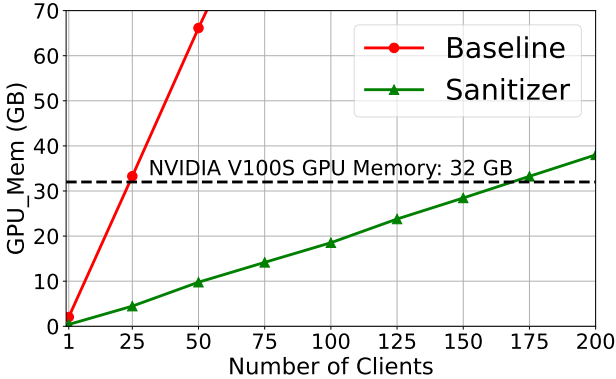


Figure 7: Sanitizer offers significantly improved scalability. It keeps GPU memory consumption (green) steadily growing but consistently below the server’s total GPU capacity of 32 GB (black) as the number of clients increases during a 10-round FL on CIFAR10 with ResNet18.

as the time required to complete sanitization skyrockets when more clients are added. In contrast, Sanitizer exhibits robust scalability across the entire range of clients tested. As shown by the green line, Sanitizer’s time complexity remains consistently low (below 1000 seconds) when scaling from 1 to 150 clients and shows only a moderate linear increase as the number of clients approaches 200. Under the fixed server’s GPU memory, the divergence between the two methods, which initially is fivefold, continues to increase progressively. The stark contrast in time consumption suggests that the improved designs we introduce into Sanitizer allow it to effectively alleviate the severe server-side computation overhead observed in the baseline, making it far more well-suited for real-world deployment in large-scale FL settings, where hundreds or even thousands of clients may be commonplace. Additionally, we believe that the scalability of Sanitizer is also represented in its optimization of GPU resource consumption.

Figure 7 illustrates the comparison of GPU memory consumption between the two methods under the same experimental settings. The baseline exhibits a sharp increase in GPU memory consumption as the number of clients increases. By the time it exceeds 25 clients, the baseline has already surpassed the threshold of 32 GB, a limit for the maximum capacity of the server’s GPU memory in our setting, indicating that a maximum of 25 client-submitted models can be processed concurrently on the server-side. In comparison, Sanitizer is capable of scaling the number of concurrently processed clients beyond 175 while remaining below the threshold, without imposing a significant burden on the server. This is essentially due to the reduced GPU memory consumed by a single backdoor subnet, making Sanitizer well-suited for large-scale FL applications with constrained server-side resources. To sum up, together these results provide a compelling argument for the deployment of Sanitizer in real-world FL environments with a large number of clients.

5.6. Effectiveness of Sanitizer in Different Neural Architectures

We also observe that Sanitizer remains effective across various architectures. Figure 8 reports the effectiveness of Sanitizer in the scenario with backdoor conflicts, which represents more realistic conditions. Whether applied to traditional fully connected architectures like MLP, classical convolutional architectures such as ResNet18, or lightweight architectures like MobileNetV3, Sanitizer consistently achieves a near-perfect WDR of over 98%, demonstrating its ability to reliably confine the watermarks to a harmless and client-specific input subspace and enable the triggering of counter-intuitive model behavior for contribution demonstration in unharmed, non-conflicting ways. The ASR is reduced from a relatively elevated level to that of random guessing, underscoring that Sanitizer can effectively neutralize malicious backdoors. Additionally, the model’s fidelity is largely preserved, with the ACC typically remaining high. Taken together, this analysis further reveals that Sanitizer is a versatile method that can be effectively applied to different neural architectures in FL.

5.7. Evaluation with Different Variants

We further investigate the impact of different variants (e.g., hyperparameters and configuration parameters) on the performance of Sanitizer, as well as its sensitivity to the changes in them. Our ablation studies mainly examine the effectiveness and efficiency of Sanitizer under two key factors in our setting: (i) varying numbers of reverse engineering epochs per round and (ii) different backdoor subnet sizes. For each factor, we only vary this single factor while keeping all other setups consistent with the default setting of the evaluation in Section 5.2. All the ablation experiments in this subsection are performed on CIFAR10 using ResNet18.

Impact of Different Round-spread Reverse Engineering Epochs on Efficiency. As shown in Figure 9, we investigate the metrics about efficiency across different round-spread reverse engineering epochs per round: (i) the GPU Mem (MB) consumed for processing a single client-submitted model during server-side operations, and (ii) the average Time (seconds) required for server-side operations per round. We also report the baseline values under the same settings for reference. These values are fixed, as the baseline does not involve the two parameters. According to the results, GPU memory utilization remains consistent, ranging from approximately 190 MB to 194 MB across all epoch settings, which is notably lower than the baseline. This stability suggests that GPU memory usage of Sanitizer is insensitive to the number of reverse engineering epochs per round. On the other hand, the time required for server-side operations per round shows a clear upward trend, escalating from 19.44 seconds at 1 epoch to 28.12 seconds at 2 epochs, and further rising to 53.73 seconds at 4 epochs. Such a trajectory in the figures stems from the inherently positive relationship between time and the number of reverse engineering epochs per round. Obviously, it persistently remains below the baseline value under varying epochs. The results show that reducing the number of round-spread reverse engineering epochs

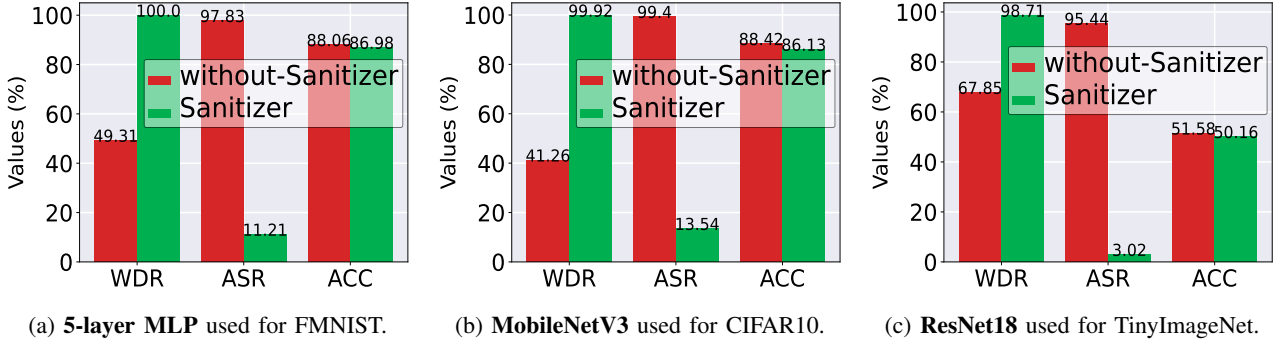


Figure 8: WDR, ASR, and ACC of Sanitizer across different architectures under the practical scenario with conflicts.

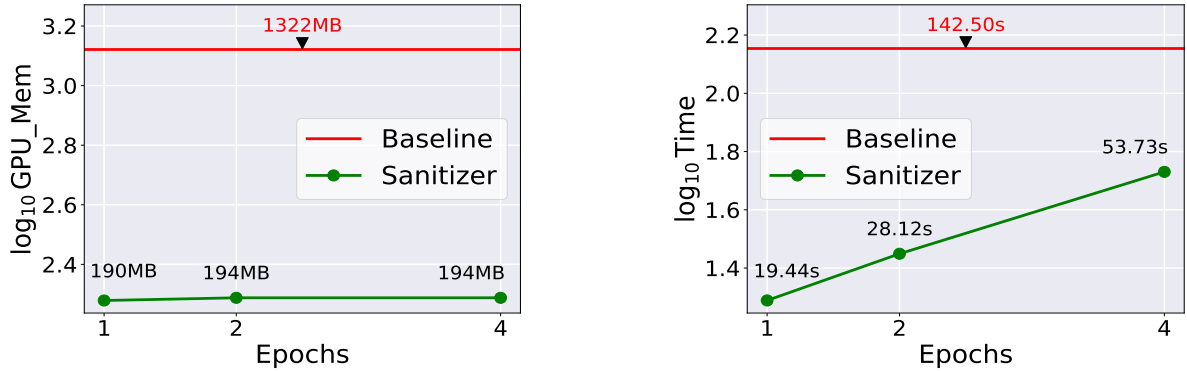


Figure 9: Efficiency metrics across different settings of round-spread reverse engineering epochs.

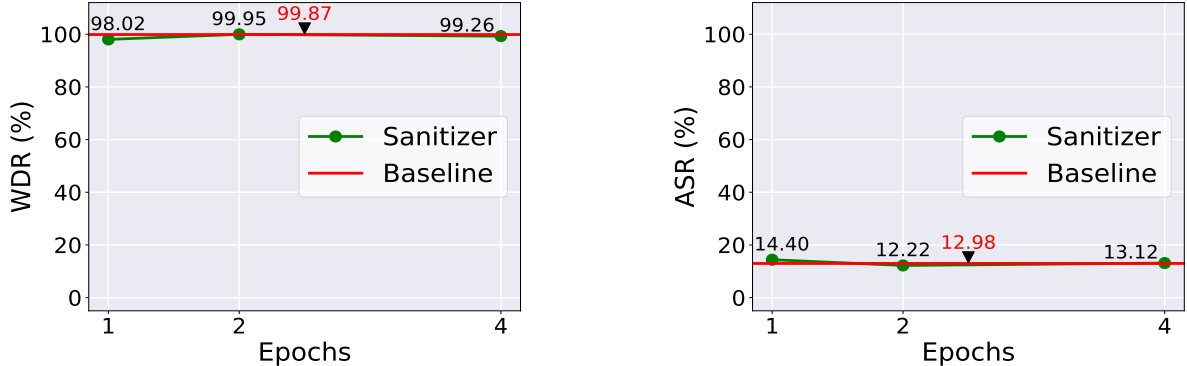


Figure 10: Effectiveness metrics across different settings of round-spread reverse engineering epochs.

can save the server-side operation time, further validating Sanitizer’s optimization for efficiency.

Impact of Different Round-spread Reverse Engineering Epochs on Effectiveness. As illustrated in Figure 10, we investigate the WDR and the ASR under different reverse engineering epochs per round. Specifically, both the baseline and Sanitizer consistently maintain a robust and near-perfect WDR over the set of epochs $\{1, 2, 4\}$. The ASR follows a similar trend, showing a slight and routine difference between the two approaches and remaining stable as the number of epochs varies. Results in this experiment confirm that different round-spread reverse engineering epochs have virtually no impact on the Sanitizer, which remains effective for any value of this factor. This shows that the effectiveness of Sanitizer is not sensitive to the number of round-spread reverse engineering epochs. In light of the aforementioned

analysis pertaining to efficiency and effectiveness, it can be concluded that, even though Sanitizer achieves comparable effectiveness to the baseline varying epochs, the latter is associated with significantly higher costs.

Impact of Different Backdoor Subnet Sizes on Efficiency. Figure 11 reports the results. Our primary objective is to investigate the relationship of efficiency between the backdoor subnet size and the key efficiency metrics. Sanitizer exhibits an increasing trend in both GPU memory utilization and required process time as the backdoor subnet size grows. In particularly, the GPU memory rises from 117 MB to 379 MB, and the process time per round extends from 16.80 to 38.90 seconds. All of these results largely outperform the baseline, demonstrating the intention behind the design of Sanitizer, which aims to enhance efficiency by reducing the size of the extracted backdoor subnet.

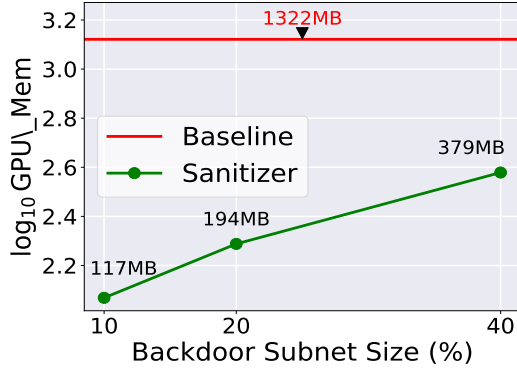


Figure 11: Efficiency metrics across different settings of the backdoor subnet size (%).

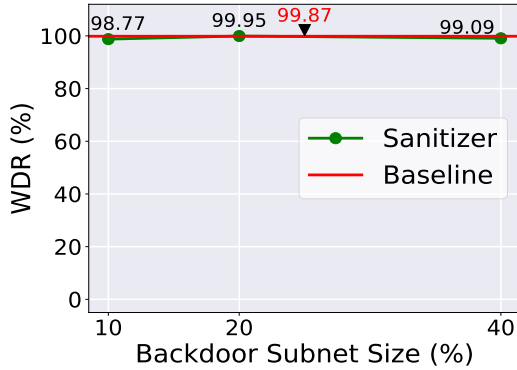


Figure 12: Effectiveness metrics across different settings of the backdoor subnet size (%).

Impact of Different Backdoor Subnet Sizes on Effectiveness. Similarly, we systematically vary the backdoor subnet size across three configurations: 10%, 20%, and 40%, and investigate the impact of them on the effectiveness of Sanitizer, keeping other variables constant to ensure fairness in comparisons. Figure 12 presents the WDR results as the backdoor subnet size increases. Sanitizer achieves a near-perfect WDR of 98.77% at the smallest backdoor subnet size (10%) and maintains a high WDR across all configurations of larger subnet sizes (20% and 40%). As for the ASR, Sanitizer shows a much lower ASR than the baseline and a stable trend across three subnet sizes. Hence, while markedly reducing resource and time consumption, Sanitizer achieves comparable performance to the baseline across different backdoor subnet sizes, demonstrating its effectiveness in eliminating harmful backdoor knowledge and enabling contribution demonstration via our unharmed watermarks. In summary, the effectiveness of Sanitizer is not sensitive to the reduction in subnet size brought about by the need to improve efficiency during the FL process.

6. Conclusions

With the goal of strengthening trustworthy federated learning, we have introduced Sanitizer, a novel and efficient sanitization approach designed to address the harmful effects and conflict issues posed by backdoor-based client-side watermarks for contribution demonstration in practical FL applications. Sanitizer leverages backdoor subnets and round-spread reverse engineering to efficiently reverse the backdoor triggers, then confines them

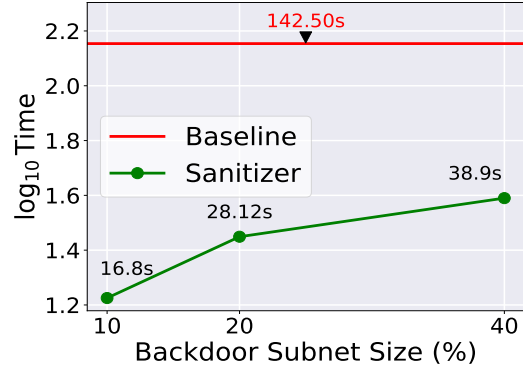


Figure 11: Efficiency metrics across different settings of the backdoor subnet size (%).

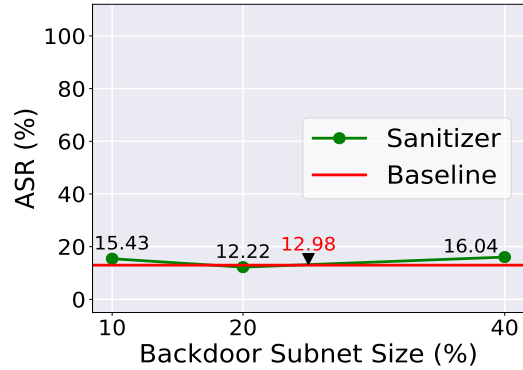


Figure 12: Effectiveness metrics across different settings of the backdoor subnet size (%).

to their own unharmed, client-specific environment before deployment and eventually makes the watermarks function in unharmed ways to successfully verify the contributions. Empirical experiments have demonstrated the effectiveness, harmlessness, and especially the efficiency of Sanitizer. We advocate for further exploration in this direction and believe that Sanitizer will inspire more advanced work for better IP protection in various real-world applications.

References

- [1] B. McMahan, E. Moore, D. Ramage, S. Hampson, and B. A. y Arcas, “Communication-efficient learning of deep networks from decentralized data,” in *Artificial intelligence and statistics*. PMLR, 2017, pp. 1273–1282.
- [2] F. Tramèr, F. Zhang, A. Juels, M. K. Reiter, and T. Ristenpart, “Stealing machine learning models via prediction {APIs},” in *25th USENIX security symposium (USENIX Security 16)*, 2016, pp. 601–618.
- [3] C.-T. Liu, C.-Y. Wang, S.-Y. Chien, and S.-H. Lai, “Fedfr: Joint optimization federated framework for generic and personalized face recognition,” in *Proceedings of the AAAI Conference on Artificial Intelligence*, vol. 36, no. 2, 2022, pp. 1656–1664.
- [4] S. Bibikar, H. Vikalo, Z. Wang, and X. Chen, “Federated dynamic sparse training: Computing less, communicating less, yet learning better,” in *Proceedings of the AAAI Conference on Artificial Intelligence*, vol. 36, no. 6, 2022, pp. 6080–6088.
- [5] D. Shenaj, E. Fanì, M. Toldo, D. Calderola, A. Tavera, U. Michieli, M. Ciccone, P. Zanuttigh, and B. Caputo, “Learning across domains and devices: Style-driven source-free domain adaptation in clustered federated learning,” in *Proceedings of the IEEE/CVF winter conference on applications of computer vision*, 2023, pp. 444–454.

[6] S. Jain and K. R. Jeripothula, "Federated learning for commercial image sources," in *Proceedings of the IEEE/CVF Winter Conference on Applications of Computer Vision (WACV)*, January 2023, pp. 6534–6543.

[7] F. Granqvist, M. Seigel, R. Van Dalen, A. Cahill, S. Shum, and M. Paulik, "Improving on-device speaker verification using federated learning with privacy," *arXiv preprint arXiv:2008.02651*, 2020.

[8] Q. Yang, A. Huang, L. Fan, C. S. Chan, J. H. Lim, K. W. Ng, D. S. Ong, and B. Li, "Federated learning with privacy-preserving and model ip-right-protection," *Machine Intelligence Research*, vol. 20, no. 1, pp. 19–37, 2023.

[9] B. Li, L. Fan, H. Gu, J. Li, and Q. Yang, "Fedipr: Ownership verification for federated deep neural network models," *IEEE Transactions on Pattern Analysis and Machine Intelligence*, vol. 45, no. 4, pp. 4521–4536, 2022.

[10] E. Bagdasaryan, A. Veit, Y. Hua, D. Estrin, and V. Shmatikov, "How to backdoor federated learning," in *International conference on artificial intelligence and statistics*. PMLR, 2020, pp. 2938–2948.

[11] W. Yang, S. Shao, Y. Yang, X. Liu, X. Liu, Z. Xia, G. Schaefer, and H. Fang, "Watermarking in secure federated learning: A verification framework based on client-side backdooring," *ACM Transactions on Intelligent Systems and Technology*, vol. 15, no. 1, pp. 1–25, 2023.

[12] G. Singh, V. Violi, and M. Fischella, "Federated learning to safeguard patients data: A medical image retrieval case," *Big Data and Cognitive Computing*, vol. 7, no. 1, p. 18, 2023.

[13] M. Lansari, R. Bellafqira, K. Kapusta, V. Thouvenot, O. Bettan, and G. Coatrieux, "When federated learning meets watermarking: A comprehensive overview of techniques for intellectual property protection," *Machine Learning and Knowledge Extraction*, vol. 5, no. 4, pp. 1382–1406, 2023.

[14] S. Yu, J. Hong, Y. Zeng, F. Wang, R. Jia, and J. Zhou, "Who leaked the model? tracking ip infringers in accountable federated learning," *arXiv preprint arXiv:2312.03205*, 2023.

[15] X. Liu, S. Shao, Y. Yang, K. Wu, W. Yang, and H. Fang, "Secure federated learning model verification: A client-side backdoor triggered watermarking scheme," in *2021 IEEE International Conference on Systems, Man, and Cybernetics (SMC)*. IEEE, 2021, pp. 2414–2419.

[16] T. Gu, K. Liu, B. Dolan-Gavitt, and S. Garg, "Badnets: Evaluating backdooring attacks on deep neural networks," *IEEE Access*, vol. 7, pp. 47 230–47 244, 2019.

[17] S. Shao, W. Yang, H. Gu, Z. Qin, L. Fan, and Q. Yang, "Fedtracker: Furnishing ownership verification and traceability for federated learning model," *IEEE Transactions on Dependable and Secure Computing*, 2024.

[18] S. Shao, Y. Li, H. Yao, Y. He, Z. Qin, and K. Ren, "Explanation as a watermark: Towards harmless and multi-bit model ownership verification via watermarking feature attribution," *arXiv preprint arXiv:2405.04825*, 2024.

[19] V. Shejwalkar, A. Houmansadr, P. Kairouz, and D. Ramage, "Back to the drawing board: A critical evaluation of poisoning attacks on production federated learning," in *2022 IEEE Symposium on Security and Privacy (SP)*. IEEE, 2022, pp. 1354–1371.

[20] A. McCartney, "Gartner top 10 strategic technology trends for 2024," <https://www.gartner.com/en/articles/gartner-top-10-strategic-technology-trends-for-2024>, accessed: 2023-10-16.

[21] F. Regazzoni, P. Palmieri, F. Smailbegovic, R. Cammarota, and I. Polian, "Protecting artificial intelligence ips: a survey of watermarking and fingerprinting for machine learning," *CAAI Transactions on Intelligence Technology*, vol. 6, no. 2, pp. 180–191, 2021.

[22] M. Xue, Y. Zhang, J. Wang, and W. Liu, "Intellectual property protection for deep learning models: Taxonomy, methods, attacks, and evaluations," *IEEE Transactions on Artificial Intelligence*, vol. 3, no. 6, pp. 908–923, 2021.

[23] Y. Uchida, Y. Nagai, S. Sakazawa, and S. Satoh, "Embedding watermarks into deep neural networks," in *Proceedings of the 2017 ACM on international conference on multimedia retrieval*, 2017, pp. 269–277.

[24] L. Fan, K. W. Ng, and C. S. Chan, "Rethinking deep neural network ownership verification: Embedding passports to defeat ambiguity attacks," *Advances in neural information processing systems*, vol. 32, 2019.

[25] B. Darvish Rouhani, H. Chen, and F. Koushanfar, "Deepsigns: An end-to-end watermarking framework for ownership protection of deep neural networks," in *Proceedings of the twenty-fourth international conference on architectural support for programming languages and operating systems*, 2019, pp. 485–497.

[26] J. Zhang, D. Chen, J. Liao, W. Zhang, G. Hua, and N. Yu, "Passport-aware normalization for deep model protection," *Advances in Neural Information Processing Systems*, vol. 33, pp. 22 619–22 628, 2020.

[27] H. Chen, B. D. Rouhani, C. Fu, J. Zhao, and F. Koushanfar, "Deepmarks: A secure fingerprinting framework for digital rights management of deep learning models," in *Proceedings of the 2019 on International Conference on Multimedia Retrieval*, 2019, pp. 105–113.

[28] Y. Adi, C. Baum, M. Cisse, B. Pinkas, and J. Keshet, "Turning your weakness into a strength: Watermarking deep neural networks by backdooring," in *27th USENIX security symposium (USENIX Security 18)*, 2018, pp. 1615–1631.

[29] J. Guo and M. Potkonjak, "Watermarking deep neural networks for embedded systems," in *2018 IEEE/ACM International Conference on Computer-Aided Design (ICCAD)*. IEEE, 2018, pp. 1–8.

[30] J. Zhang, Z. Gu, J. Jang, H. Wu, M. P. Stoecklin, H. Huang, and I. Molloy, "Protecting intellectual property of deep neural networks with watermarking," in *Proceedings of the 2018 on Asia conference on computer and communications security*, 2018, pp. 159–172.

[31] Z. Li, C. Hu, Y. Zhang, and S. Guo, "How to prove your model belongs to you: A blind-watermark based framework to protect intellectual property of dnn," in *Proceedings of the 35th annual computer security applications conference*, 2019, pp. 126–137.

[32] E. Le Merrer, P. Perez, and G. Trédan, "Adversarial frontier stitching for remote neural network watermarking," *Neural Computing and Applications*, vol. 32, no. 13, pp. 9233–9244, 2020.

[33] J. Liang and R. Wang, "Fedcip: Federated client intellectual property protection with traitor tracking," *arXiv preprint arXiv:2306.01356*, 2023.

[34] B. G. Tekgul, Y. Xia, S. Marchal, and N. Asokan, "Waffle: Watermarking in federated learning," in *2021 40th International Symposium on Reliable Distributed Systems (SRDS)*. IEEE, 2021, pp. 310–320.

[35] W. Yang, G. Zhu, Y. Yin, H. Gu, L. Fan, Q. Yang, and X. Cao, "Fedsov: federated model secure ownership verification with unforgeable signature," *arXiv preprint arXiv:2305.06085*, 2023.

[36] A. Benaissa, B. Retiat, B. Cebere, and A. E. Belfedhal, "Tenseal: A library for encrypted tensor operations using homomorphic encryption," *arXiv preprint arXiv:2104.03152*, 2021.

[37] F.-Q. Li, S.-L. Wang, and A. W.-C. Liew, "Merkle-sign: Watermarking framework for deep neural networks in federated learning," 2021.

[38] W. Yang, Y. Yin, G. Zhu, H. Gu, L. Fan, X. Cao, and Q. Yang, "Fedzkp: Federated model ownership verification with zero-knowledge proof," *arXiv preprint arXiv:2305.04507*, 2023.

[39] Y. Aono, T. Hayashi, L. Wang, S. Moriai *et al.*, "Privacy-preserving deep learning via additively homomorphic encryption," *IEEE transactions on information forensics and security*, vol. 13, no. 5, pp. 1333–1345, 2017.

[40] Y. Xu, Y. Tan, C. Zhang, K. Chi, P. Sun, W. Yang, J. Ren, H. Jiang, and Y. Zhang, "Robwe: Robust watermark embedding for personalized federated learning model ownership protection," *arXiv preprint arXiv:2402.19054*, 2024.

[41] C. Xie, K. Huang, P.-Y. Chen, and B. Li, "Dba: Distributed backdoor attacks against federated learning," in *International conference on learning representations*, 2019.

[42] K. Bonawitz, V. Ivanov, B. Kreuter, A. Marcedone, H. B. McMahan, S. Patel, D. Ramage, A. Segal, and K. Seth, “Practical secure aggregation for privacy-preserving machine learning,” in *proceedings of the 2017 ACM SIGSAC Conference on Computer and Communications Security*, 2017, pp. 1175–1191.

[43] X. Xu, K. Huang, Y. Li, Z. Qin, and K. Ren, “Towards reliable and efficient backdoor trigger inversion via decoupling benign features,” in *The Twelfth International Conference on Learning Representations*, 2023.

[44] X. Cao, M. Fang, J. Liu, and N. Z. Gong, “Fltrust: Byzantine-robust federated learning via trust bootstrapping,” in *ISOC Network and Distributed System Security Symposium (NDSS)*, 2021.

[45] Z. Wang, K. Mei, H. Ding, J. Zhai, and S. Ma, “Rethinking the reverse-engineering of trojan triggers,” *Advances in Neural Information Processing Systems*, vol. 35, pp. 9738–9753, 2022.

[46] J. Jia, Z. Yuan, D. Sahabandu, L. Niu, A. Rajabi, B. Ramasubramanian, B. Li, and R. Poovendran, “Fedgame: a game-theoretic defense against backdoor attacks in federated learning,” *Advances in Neural Information Processing Systems*, vol. 36, 2024.

[47] P. Kairouz, H. B. McMahan, B. Avent, A. Bellet, M. Bennis, A. N. Bhagoji, K. Bonawitz, Z. Charles, G. Cormode, R. Cummings *et al.*, “Advances and open problems in federated learning,” *Foundations and trends® in machine learning*, vol. 14, no. 1–2, pp. 1–210, 2021.

[48] Y. Gao, B. G. Doan, Z. Zhang, S. Ma, J. Zhang, A. Fu, S. Nepal, and H. Kim, “Backdoor attacks and countermeasures on deep learning: A comprehensive review,” *arXiv preprint arXiv:2007.10760*, 2020.

[49] B. Wang, Y. Yao, S. Shan, H. Li, B. Viswanath, H. Zheng, and B. Y. Zhao, “Neural cleanse: Identifying and mitigating backdoor attacks in neural networks,” in *2019 IEEE symposium on security and privacy (SP)*. IEEE, 2019, pp. 707–723.

[50] X. Liu, F. Li, B. Wen, and Q. Li, “Removing backdoor-based watermarks in neural networks with limited data,” in *2020 25th International Conference on Pattern Recognition (ICPR)*. IEEE, 2021, pp. 10 149–10 156.

[51] K. Zhang, G. Tao, Q. Xu, S. Cheng, S. An, Y. Liu, S. Feng, G. Shen, P.-Y. Chen, S. Ma *et al.*, “Flip: A provable defense framework for backdoor mitigation in federated learning,” *arXiv preprint arXiv:2210.12873*, 2022.

[52] H. Wang, J. Hong, A. Zhang, J. Zhou, and Z. Wang, “Trap and replace: Defending backdoor attacks by trapping them into an easy-to-replace subnetwork,” *Advances in neural information processing systems*, vol. 35, pp. 36 026–36 039, 2022.

[53] R. Tang, M. Du, N. Liu, F. Yang, and X. Hu, “An embarrassingly simple approach for trojan attack in deep neural networks,” in *Proceedings of the 26th ACM SIGKDD international conference on knowledge discovery & data mining*, 2020, pp. 218–228.

[54] X. Qi, T. Xie, R. Pan, J. Zhu, Y. Yang, and K. Bu, “Towards practical deployment-stage backdoor attack on deep neural networks,” in *Proceedings of the IEEE/CVF Conference on Computer Vision and Pattern Recognition*, 2022, pp. 13 347–13 357.

[55] C. Lakshminarayanan and A. Vikram Singh, “Neural path features and neural path kernel: Understanding the role of gates in deep learning,” *Advances in Neural Information Processing Systems*, vol. 33, pp. 5227–5237, 2020.

[56] X. Qi, J. Zhu, C. Xie, and Y. Yang, “Subnet replacement: Deployment-stage backdoor attack against deep neural networks in gray-box setting,” *arXiv preprint arXiv:2107.07240*, 2021.

[57] Y. Li, X. Lyu, X. Ma, N. Koren, L. Lyu, B. Li, and Y.-G. Jiang, “Reconstructive neuron pruning for backdoor defense,” in *International Conference on Machine Learning*. PMLR, 2023, pp. 19 837–19 854.

[58] X. Qi, T. Xie, J. T. Wang, T. Wu, S. Mahloujifar, and P. Mittal, “Towards a proactive {ML} approach for detecting backdoor poison samples,” in *32nd USENIX Security Symposium (USENIX Security 23)*, 2023, pp. 1685–1702.

[59] T. Xie, X. Qi, P. He, Y. Li, J. T. Wang, and P. Mittal, “Badexpert: Extracting backdoor functionality for accurate backdoor input detection,” in *The Twelfth International Conference on Learning Representations*, 2024.

[60] C. Wu, X. Yang, S. Zhu, and P. Mitra, “Toward cleansing backdoored neural networks in federated learning,” in *2022 IEEE 42nd International Conference on Distributed Computing Systems (ICDCS)*. IEEE, 2022, pp. 820–830.

[61] K. Liu, B. Dolan-Gavitt, and S. Garg, “Fine-pruning: Defending against backdooring attacks on deep neural networks,” in *International symposium on research in attacks, intrusions, and defenses*. Springer, 2018, pp. 273–294.

[62] M. Zhu, S. Wei, L. Shen, Y. Fan, and B. Wu, “Enhancing fine-tuning based backdoor defense with sharpness-aware minimization,” in *Proceedings of the IEEE/CVF International Conference on Computer Vision*, 2023, pp. 4466–4477.

[63] Y. Yao, H. Li, H. Zheng, and B. Y. Zhao, “Latent backdoor attacks on deep neural networks,” in *Proceedings of the 2019 ACM SIGSAC conference on computer and communications security*, 2019, pp. 2041–2055.

[64] X. Han, K. Rasul, and R. Vollgraf, “Fashion-mnist: a novel image dataset for benchmarking machine learning algorithms,” *arXiv: Learning*, Aug 2017.

[65] A. Krizhevsky, G. Hinton *et al.*, “Learning multiple layers of features from tiny images,” 2009.

[66] Y. Le and X. Yang, “Tiny imagenet visual recognition challenge,” *CS 231N*, vol. 7, no. 7, p. 3, 2015.

[67] K. He, X. Zhang, S. Ren, and J. Sun, “Deep residual learning for image recognition,” in *Proceedings of the IEEE conference on computer vision and pattern recognition*, 2016, pp. 770–778.

[68] A. Howard, M. Sandler, G. Chu, L.-C. Chen, B. Chen, M. Tan, W. Wang, Y. Zhu, R. Pang, V. Vasudevan *et al.*, “Searching for mobilenetv3,” in *Proceedings of the IEEE/CVF international conference on computer vision*, 2019, pp. 1314–1324.

[69] K.-H. Chow, L. Liu, W. Wei, F. Ilhan, and Y. Wu, “Stdlns: Model hijacking-resilient federated learning for object detection,” in *Proceedings of the IEEE/CVF Conference on Computer Vision and Pattern Recognition*, 2023, pp. 16 343–16 351.

[70] M. Zink, D. Irwin, E. Cecchet, H. Saplakoglu, O. Krieger, M. Herbordt, M. Daitzman, P. Desnoyers, M. Leeser, and S. Handagala, “The open cloud testbed (oct): A platform for research into new cloud technologies,” in *2021 IEEE 10th International Conference on Cloud Networking (CloudNet)*. IEEE, 2021, pp. 140–147.

Appendix A. Outline of Supplementary Materials

This part serves as the appendix, providing additional details for our main paper. It is organized as follows:

- **Section A.1:** Data Availability Statements.
- **Section A.2:** The Algorithm of Sanitizer.
- **Section A.3:** Default Parameter Setting.
- **Section A.4:** More Details on the Extracted Backdoor Subnet.
- **Section A.5:** Visual Examples of Trigger Inversion on the FL-trained Model without Sanitizer.
- **Section A.6:** More Analysis and Discussion.
- **Section A.7:** Limitation and Future Work.

A.1. Data Availability Statements

We fully support the principles of open science, aiming to promote transparency, reproducibility, and collaborative research. The datasets (Fashion-MNIST (FMNIST) [64], CIFAR10 [65], and TinyImageNet [66]) used in this study are publicly available and widely recognized as the benchmark in the image classification tasks. The details of these datasets are as follows:

Algorithm 1 The Baseline method (Left) vs. Our Sanitizer (Right). The main difference is the ▷ Green Line.

Input: Total communication rounds of FL T ; Number of clients K ; Defense data $(x_d, y_d) \in \mathcal{D}_d$; Unharmful data $x_u \in \mathcal{D}_u$; Poisoning rate of backdoor embedding $\rho\%$;
Output: Unharmful Watermarked FL-trained Model $\mathcal{F}(\theta_*)$.

- 1: Server sends θ_{global}^0 to all K clients for initialization.
- 2: **for** each round $t = 0, 1, \dots, T - 1$ **do**
- 3: /* Client-Side */
- 4: **for** each client $k = 0, 1, \dots, K - 1$ in parallel **do**
- 5: Client k trains a backdoored model $f(\theta_k)$ via Equation 1 on $\rho\%$.
- 6: **end for**
- 7: /* Server-Side */
- 8: **for** each $f(\theta_k)$, $k = 0, 1, \dots, K - 1$ in parallel **do**
- 9: Conduct full Reverse Engineering on $f(\theta_k)$ for trigger pattern Δ_k recovery and target class y_t^k detection via Equation 4. ▷ Trigger Recovery.
- 10: **end for**
- 11: Aggregation.
- 12: **end for**
- 13: Server conducts $\max \mathbb{E}_{(x_d, y_d) \in \mathcal{D}_d} \mathcal{L}(f(x_d + \Delta; \theta), y_t)$ on FL-trained Model $\mathcal{F}(\theta)$. ▷ Unlearning.
- 14: Server conducts $\min \mathbb{E}_{(x_d, y_d) \in \mathcal{D}_d} \mathcal{L}(f(x_d + \Delta; \theta), y_d)$ and $\min \mathbb{E}_{x_u \in \mathcal{D}_u} \mathcal{L}(f(x_u + \Delta; \theta), y_t)$ on FL-trained Model $\mathcal{F}(\theta)$. ▷ Relearning.
- 15: **return** Unharmful Watermarked FL-trained Model $\mathcal{F}(\theta_*)$.

Input: Total communication rounds of FL T ; Number of clients K ; Defense data $(x_d, y_d) \in \mathcal{D}_d$; Unharmful data $x_u \in \mathcal{D}_u$; Size of backdoor subnet $s\%$; Epoch of round-spread reverse engineering per round e ; Poisoning rate of backdoor embedding $\rho\%$;
Output: Unharmful Watermarked FL-trained Model $\mathcal{F}(\theta_*)$.

- 1: Server sends θ_{global}^0 to all K clients for initialization.
- 2: **for** each round $t = 0, 1, \dots, T - 1$ **do**
- 3: /* Client-Side */
- 4: **for** each client $k = 0, 1, \dots, K - 1$ in parallel **do**
- 5: Client k trains a backdoored model $f(\theta_k)$ via Equation 1 on $\rho\%$.
- 6: **end for**
- 7: /* Server-Side */
- 8: **for** each $f(\theta_k)$, $k = 0, 1, \dots, K - 1$ in parallel **do**
- 9: ▷ Conduct Clean Unlearning on $f(\theta_k)$ with (x_d, y_d) by Equation 2 to obtain $f(\theta'_k)$.
- 10: ▷ Identify and extract a backdoor subnet $f_s(\theta'_k)$ from $f(\theta_k)$ of Top $s\%$ UWC via Equation 3.
- 11: ▷ Conduct round-spread reverse engineering for e epochs on $f_s(\theta'_k)$ for trigger pattern Δ_k and target class y_t^k and pruning for aggregation.
- 12: **end for**
- 13: Aggregation by Equation 5.
- 14: **end for**
- 15: Server conducts Unharmful Relearning on FL-trained Model $\mathcal{F}(\theta)$ via Equation 7.
- 16: **return** Unharmful Watermarked FL-trained Model $\mathcal{F}(\theta_*)$.

- **FashionMNIST:** Fashion-MNIST contains 70,000 28x28 grayscale images across 10 fashion categories. The dataset is split into 60,000 training images and 10,000 test images. FashionMNIST is designed as a modern alternative to the classic MNIST dataset. It can be accessed from <https://github.com/zalandoresearch/fashion-mnist>. It is supported natively by PyTorch and will be downloaded automatically.
- **CIFAR-10:** CIFAR10 consists of 60,000 32x32 color images in 10 different classes. The dataset is divided into 50,000 training images and 10,000 test images, and is widely used for evaluating machine learning models on small-scale object recognition tasks. It is publicly available at <http://www.cs.toronto.edu/~kriz/cifar.html>. It is supported natively by PyTorch and will be downloaded automatically.
- **TinyImageNet:** TinyImageNet includes 100,000 64x64 color images across 200 classes. Each class contains 500 training images and 50 validation images. TinyImageNet is a smaller, more manageable subset of the full ImageNet dataset, commonly used for evaluating deep learning models. It can be downloaded from <http://cs231n.stanford.edu/tiny-imagenet-200.zip>.

A.2. The Algorithm of Sanitizer

In Algorithm 1, we present the algorithmic details that we introduce in Section 4. We describe the baseline method as well as Sanitizer in full. The baseline employs a naive sanitization method, which, while effective to some extent, suffers from unacceptable inefficiency. This limitation motivated the development of our proposed Sanitizer. By maintaining the sanitization effectiveness, Sanitizer significantly reduces unnecessary overhead, leading to noticeable improvements in both processing time and GPU memory consumption. These optimizations make it a far more practical solution in scenarios requiring both efficiency and effectiveness.

A.3. Default Parameter Setting

Table 5 summarizes the default parameter setting in our empirical evaluation.

A.4. More Details on the Extracted Backdoor Subnet

Based on the default settings, we present a further analysis of the extracted backdoor subnet in two different architectures when applied to CIFAR10, which has a resolution of 32×32 pixels and three color channels (RGB). As shown in Table 6, we compared the number of parameters

Module	Parameter	Setting
Client-side Training Process	communication rounds	100
	local training epochs	5
	local training batch size	128
	local learning rate	0.05
	optimizer	SGD
	momentum	0.9
	weight decay	5e-4
	backdoor poisoning rate	0.1
Clean Unlearning	defense data rate	0.05
	clean unlearning epochs	10
	clean unlearning batch size	128
	learning rate	0.01
	early stop threshold	0.15
Round-spread Reverse Engineering	backdoor subnet size rate	0.2
	round-spread epochs	2
	batch size	128
	learning rate	0.2
	weight for L1 norm of mask	0.01
Unharmful Relearning	relearning epochs	50
	batch size	64
	learning rate	0.005
	weight for clean objective	0.8
	weight for unharmful objective	0.2

Table 5: Default Parameter Setting in FL with Sanitizer.

and FLOPs between the original network and the extracted backdoor subnet. The results clearly demonstrate a significant reduction in computational complexity. This decrease in model size and operations highlights the efficiency gained through subnet extraction, making it more suitable for resource-constrained environments without sacrificing key performance metrics.

A.5. Visual Examples of Trigger Inversion on the FL-trained Model without Sanitizer

We observe that recovering the trigger from an FL-trained model without employing Sanitizer appears to be not feasible. In this scenario, no defense mechanisms are applied during the training phase of the existing backdoor-based client-side watermarked FL, and reverse engineering is only performed on the final FL-trained model after the FL process has completed, prior to deployment. Table 7 illustrates that the shortcut, or trigger, associated with each class cannot be successfully recovered in the final FL-trained model. We conjecture that this outcome may be attributed to the aggregation process, which potentially dilutes the backdoor effect, thereby obscuring the true trigger. This dilution likely results from the averaging of model updates across clients, which disperses the influence of individual backdoor triggers and diminishes their impact on the global model. Consequently, the aggregated model fails to retain the malicious characteristics necessary for trigger identification. The results indicate that it seems not possible to recover the specific triggers associated with each target label, highlighting the difficulty of accurately identifying and extracting the embedded backdoors under this condition.

Table 6: Complexity of the extracted backdoor subnet in two different architectures when applied to CIFAR10.

Network	CIFAR10 & ResNet18	
	#Params	FLOPs
Original Network	11.17M	1.116G
Backdoor Subnet	444.22K	43.677M

Network	CIFAR10 & MobileNetV3	
	#Params	FLOPs
Original Network	1.684M	5.145M
Backdoor Subnet	80.821K	336.630K

Table 7: The Original Trigger corresponding to each class and its recovered version.

	Class 1	Class 2	Class 3
Original Trigger			
Reversed Version			

A.6. More Analysis and Discussion

- The number of communication rounds required to achieve both optimal ACC for the main task and successful backdoor trigger inversion is also a factor influencing the overall efficiency of FL. Reducing the round-spread reverse engineering epochs may lead to an increased number of communication rounds required to achieve the desired outcomes, and vice versa. This highlights a clear trade-off between minimizing communication rounds and optimizing server-side efficiency. This trade-off requires careful consideration to balance computational resources and performance goals effectively.
- Why assume a Badnet-style backdoor? We argue that in a scenario where FL clients co-own the jointly trained model, clients tend to embed watermarks in the simplest and most direct manner to demonstrate their contribution, obviating the need for complex and impractical techniques. As clients cannot easily break into the source code and manipulate the standard local learning, the easiest way for them to watermark the model is to conduct data poisoning backdoors. This means they don't need to expend significant effort (or resources) to demonstrate their contribution; instead, a more practical and straightforward approach for them is implementing a Badnet-like patch replacement that applies a trigger pattern onto an image and changes its label. It is reasonable to assume that they prefer to demonstrate their contribution with minimal

cost rather than utilizing more sophisticated backdoor embedding methods. Moreover, we specifically focus on Badnet-like backdoor-based watermarks, as our approach is not designed to defend against backdoors in general, but rather to serve as a safeguard when such backdoors are used as watermarks under specific conditions.

A.7. Limitation and Future Work

Sanitizer has confirmed the promising results of making the backdoor-based client-side watermarks unharful to enhance the contribution demonstration in FL, but it also comes with several limitations: (a) Sanitizer has not yet optimized the computational cost associated with subsequent step after FL, although it is relatively negligible compared to the whole FL period; (b) the feasibility of applying Sanitizer to Transformer-based architectures, such as ViT, remains unknown for now.

In the future, we will address these challenges and further extend the applicability of Sanitizer. Sanitizer represents the first research effort that directly targets the harmlessness of backdoor-based watermarks in FL. This work not only advances the state-of-the-art for image classification tasks but also paves the way for future exploration across a broader range of applications, including object detection and beyond. We anticipate that the principles behind Sanitizer can be effectively extended to other FL scenarios, driving further innovations in enhancing the IP protection and contribution demonstration of the FL-trained model.